Analyst

RSC Publishing

COMMUNICATION

View Article Online
View Journal | View Issue

Co_3O_4 microspheres with free-standing nanofibers for high performance non-enzymatic glucose sensor†

Cite this: *Analyst*, 2013, **138**, 6727

Chunyan Guo, Xuan Zhang, Huanhuan Huo, Cailing Xu* and Xu Han

Received 23rd July 2013
Accepted 25th August 2013

DOI: 10.1039/c3an01403g

www.rsc.org/analyst

Co_3O_4 microspheres with free-standing or bundled nanofibers (NFs) were fabricated for use as a platform for non-enzymatic glucose sensing. The sensor based on free-standing Co_3O_4 NFs displays enhanced sensitivity (1440 μA mM^{-1} cm^{-2}), a wider linear range (0.005–12 mM) and superior selectivity. The application of this glucose sensor in human blood serum has also been demonstrated successfully.

Glucose sensing has received continuous interest due to its wide application in biotechnology, clinical diagnostics and the food industry.[1,2] In recent years, non-enzymatic glucose sensing has been a research hotspot following enzymatic glucose sensing because it can effectively avoids the essential drawbacks suffered by enzymatic glucose sensors.[3] Many efforts have been contributed to the development of various nanostructured materials for constructing non-enzymatic glucose sensors, including precious metals (Au, Pd, Pt) and their alloys (Pt–Au, Pt–Pd), transition metals (Ni, Cu) and their oxides (NiO, CuO, Cu_2O, Co_3O_4).[3–8] Amongst these materials, nanostructured cobalt oxide has been demonstrated as a promising material for use in non-enzymatic glucose sensors, supercapacitors, lithium ion batteries, gas sensing and superhydrophobic surfaces[9–13] owing to its low cost, environmentally friendly nature and relatively good conductivity. For the first time, Ding *et al.*[14] reported the mechanism of Co_3O_4 nanofibers (NFs) towards glucose oxidation, which relies upon formation of the CoO_2/CoOOH redox pair on the working electrode surface in alkaline electrolyte media. But this Co_3O_4 NF glucose sensor only shows a sensitivity of 36.25 μA mM^{-1} cm^{-2} and a linear range up to 2.04 mM. Kung *et al.*[15] reported CoO nanorods (NRs) synthesized through chemical bath deposition for a non-enzymatic glucose sensor. Although the sensitivity of the CoO NRs has been improved to 571.8 μA mM^{-1} cm^{-2}, the linear range up to 3.5 mM is far from satisfactory. Dong *et al.*[16] prepared a 3D graphene–Co_3O_4 NF composite material as a glucose sensor. This sensor exhibits a high sensitivity up to 3.39 mA mM^{-1} cm^{-2}. However, the performance of the sensor was compromised due to its up to 80 μM linear range. According to the current limited reports on glucose sensors based on cobalt oxides, it is noticeable that the electrodes were mostly fabricated with a 1D cobalt oxide nanostructure, as the 1D nanostructure is believed to have a higher surface area than the 2D nanostructure.[17] But the common and fatal drawback of these cobalt oxide nanostructures is that the 1D structures cannot be well separated from each other. When applied as an electrode to construct glucose sensors, the random and compacted 1D material cannot be fully exploited. The spaceless connection between these 1D nanostructures provides only few channels for the transport of glucose molecules and electrolyte ions, which undoubtedly results in the low sensitivity and narrow linesr range. On the other hand, considering the sensitivity as high as 3.39 mA mM^{-1} cm^{-2} reported by Dong's group,[16] the unique structure and conductivity offered by the 3D graphene substrate, which can provide multiplexed and highly conductive pathways for the species involved in the electrocatalytic reaction, is the fundamental and profitable factor that endows the electrode with high sensitivity. Therefore, the preparation of a well-dispersed 1D cobalt oxide nanostructure on a 3D highly conductive substrate may be a more effective approach to figure out the existing problems of low sensitivity and narrow linear range for cobalt oxide-based glucose sensors.

According to our previous research, nickel foam treated with hydrochloric acid has a highly porous structure with many nanofibers on the skeleton,[18,19] and the inherent high electron conductivity and 3D network make it an ideal substrate electrode for an electrochemical biosensor.[20,21] Herein, Co_3O_4 microspheres with free-standing or bundled nanofibers were prepared by adding the surfactant of CTAB, or not, in the hydrothermal process. The 3D nickel foam treated with

Key Laboratory of Nonferrous Metal Chemistry and Resources Utilization of Gansu Province, College of Chemistry and Chemical Engineering, Lanzhou University, Lanzhou, 730000, P. R. China. E-mail: xucl@lzu.edu.cn; Fax: +86-931-891-2582; Tel: +86-931-891-2589

† Electronic supplementary information (ESI) available. See DOI: 10.1039/c3an01403g

hydrochloric acid was used as the scaffold to make full use of the active material. The 3D electrode constructed using Co_3O_4 microspheres with free-standing nanofibers shows a much better electrochemical catalytic performance towards glucose oxidation than that prepared using Co_3O_4 microspheres with bundled nanofibers. Furthermore, the excellent electrochemical performance of this novel electrode, combined with good reproducibility, inherent stability and good practical application, indicates its commercial value as a glucose sensor.

Two types of samples were prepared through a typical hydrothermal method and denoted as CTAB–Co_3O_4 and Co_3O_4, respectively. The details of the experimental are shown in the ESI.†

Fig. 1A shows the XRD patterns of the samples obtained by the hydrothermal method with and without CTAB. The two samples exhibit the similar diffraction peaks that can be perfectly indexed to the cubic Co_3O_4 phase (JCPDS: 43-1003). Except for the diffraction peaks of the Ni substrate and the Co_3O_4 phase, no other impurity peaks can be detected. Additionally, the peaks of the CTAB–Co_3O_4 sample are higher and narrower than those of the Co_3O_4 sample, demonstrating the good crystallinity of the CTAB–Co_3O_4 sample.

The morphology of the Co_3O_4 and CTAB–Co_3O_4 samples was firstly characterized by SEM. The low-magnification SEM image (Fig. 1B) of the Co_3O_4 sample exhibits a quasi-spherical appearance with a diameter of 8 μm. The high-magnification SEM image, as shown in Fig. 1C, demonstrates that the Co_3O_4 microsphere consists of lots of nanofibers, but that the nanofibers are pieced together and take the shape of many compacted clusters.

Fig. 1D and 1E show the SEM images of the CTAB–Co_3O_4 sample. Obviously, many urchin-like microspheres assembled with numerous free-standing nanofibers are formed (Fig. 1D) and the diameter of the individual microspheres increases to 9.5 μm (the inset of Fig. 1D). Meanwhile, as shown in Fig. 1E, it can clearly be seen that the nanofibers are independent of each other and provide a multichannel 3D superstructure, which is different from the structure presented in Fig. 1C. Fig. 1F and 1G show the typical TEM images of the nanofibers of Co_3O_4 and CTAB–Co_3O_4 samples, respectively. Both nanofibers consist of an amount of nanoparticles where the size of the particles obviously decreases after the addition of CTAB in the hydrothermal process. Moreover, a lot of mesopores can be seen on the surface of the two samples, which is the result of the successive release and loss of CO_2 and H_2O in the annealing process. It is believed that the excellent dispersion degree of the nanofibers in the CTAB–Co_3O_4 sample should be attributed to the stereochemical effect of CTAB.[22] The lattice spacing of 0.285 nm corresponds to the (220) crystal plane of cubic Co_3O_4, as seen from the HRTEM image (Fig. 1H), which is consistent with the XRD data. The SAED pattern (inset of Fig. 1H) demonstrates a polycrystalline structure for the CTAB–Co_3O_4 sample.

Fig. 2A presents the cyclic voltammograms (CVs) of the CTAB–Co_3O_4 and Co_3O_4 electrodes in the absence and presence of glucose in 0.5 M NaOH solution, respectively. Without glucose addition, a pair of redox peaks can be observed with the anodic peak at around 0.50 V and the cathodic peak at around 0.37 V (*vs.* Hg/HgO), which can be attributed to the redox peak of Co^{3+}/Co^{4+}. No redox pair corresponding to Co^{2+}/Co^{3+} was observed. According to the previous report the appearance of the Co^{2+}/Co^{3+} redox peak depends possibly upon factors which come either from itself or outside such as the electrolyte concentration, scan rate and the thickness of the active material.[23,24] Additionally, the anodic peak of CTAB–Co_3O_4 has a slightly more negative value than that of Co_3O_4, which implies the low polarization brought by the multiple channels for the fast transport of ions and molecules involved in the reaction. Upon addition of 1 mM glucose, an increase of the anodic peak current is observed for both electrodes, demonstrating the electrode electrocatalysis for glucose oxidation. The anodic peaks shift to a more positive value which was caused by the concentration polarization as described in our previous report.[20] However, the increase of peak current of the CTAB–Co_3O_4 electrode is much higher (3-fold) than that of the Co_3O_4 electrode, which suggests a superior catalytic activity of the CTAB–Co_3O_4 electrode to glucose oxidation. This can be explained by the fact that these free-standing 1D nanofibers in

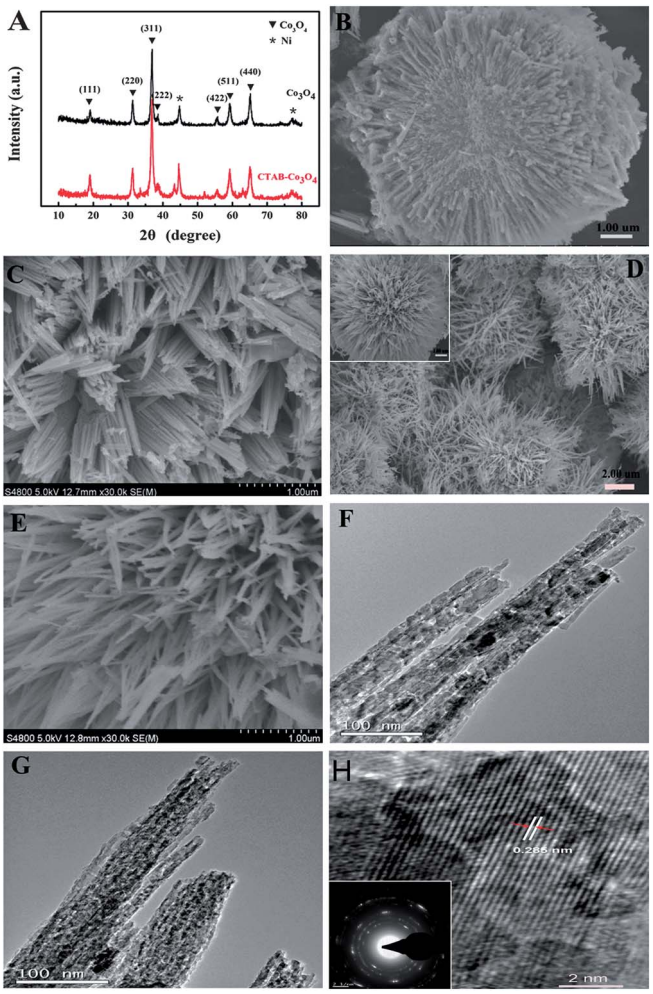

Fig. 1 (A) XRD patterns of Co_3O_4 (black line) and CTAB–Co_3O_4 (red line) samples; SEM and TEM images of (B, C and F) Co_3O_4, and (D, E and G) CTAB–Co_3O_4 samples; (H) HRTEM and SAED (inset) of CTAB–Co_3O_4.

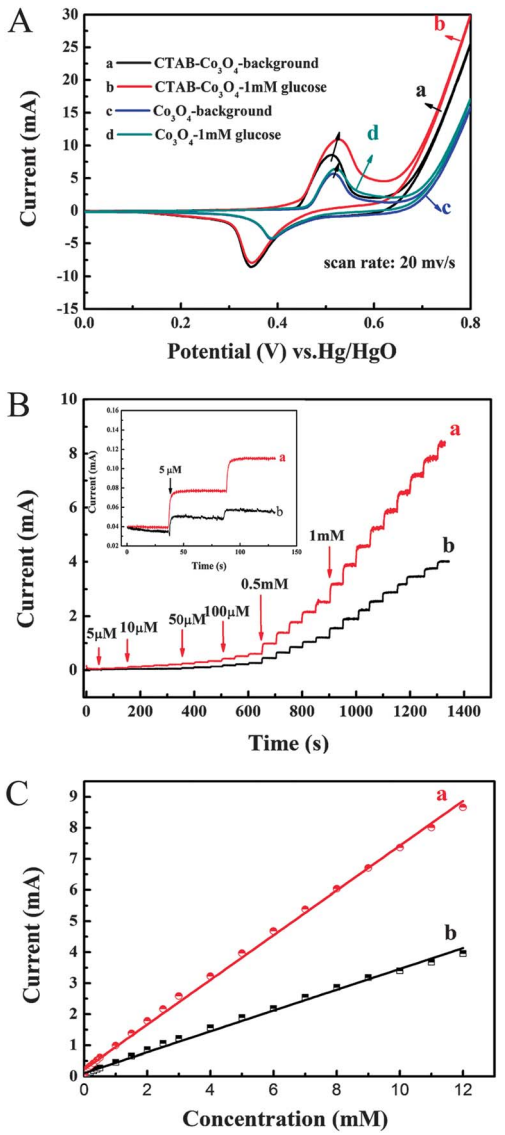

Fig. 2 (A) CVs of CTAB–Co_3O_4 (a and b) and Co_3O_4 (c and d) electrodes in the absence (a and c) and presence (b and d) of 1 mM glucose, respectively. (B) Amperometric response to successive additions of glucose obtained at the CTAB–Co_3O_4 (a) and Co_3O_4 (b) electrodes at an applied potential of 0.55 V. Inset shows the response to low-concentration glucose. (C) Corresponding calibration curves from (B).

the CTAB–Co_3O_4 electrode not only offer the critical spaces for the transport of ions but also improve the availability of the material. Additionally, to examine the synergistic effect of the nickel foam scaffold and free-standing Co_3O_4 NFs, the current response of the bare nickel foam and the glass carbon electrode (GCE) decorated with CTAB–Co_3O_4 towards glucose oxidation were also investigated, respectively. The results show that the current responses of the bare nickel foam electrode and the GCE decorated with CTAB–Co_3O_4 (Fig. S1†) are much lower (4.4-fold and 7-fold) than that of the nickel foam electrode decorated with CTAB–Co_3O_4, suggesting that the nickel foam can provide more attachment sites for Co_3O_4.

Considering that the applied potential can strongly affect the current response of the sensor, the applied potential was systemically optimized. Fig. S2† depicts the potential versus current plot of the CTAB–Co_3O_4 electrode towards 2.0 mM glucose. The result indicates that with the applied potential shifting from 0.4 to 0.65 V, the current response increases firstly and reaches a maximum at 0.55 V, then decreases when the potential exceeds 0.55 V. Therefore, 0.55 V (0.47 V *vs.* Ag/AgCl) is selected as the optimal potential in the subsequent study. This potential value is more negative than that previously reported.[14–16,25] It looks to have benefited from the enhanced contact area and large transport channels, which can assist the molecules and ions involved in the glucose oxidation of this system to approach the active sites readily, so as to effectively decrease the energy required for the reaction and accelerate the reaction dynamics. Moreover, it has been proposed that most of the interfering species such as uric acid (UA) and ascorbic acid (AA) are not active when the potential is below 0.5 V (*vs.* Ag/AgCl),[3] and thus this optimal potential will have a positive effect on improving the selectivity.

Fig. 2B compares the amperometric response of the CTAB–Co_3O_4 and Co_3O_4 electrodes at 0.55 V with successive additions of glucose. In this case, both electrodes rapidly respond to the addition of glucose at 0.55 V (*vs.* Hg/HgO), achieving 95% of the steady-current within 2 s and 3 s, respectively. And they all display a wide linear range of 0.005–12 mM. However, the sensitivity (calculated from calibration curves in Fig. 2C) of CTAB–Co_3O_4 (1440 μA mM^{-1} cm^{-2}) is 2.1-fold greater than that of Co_3O_4 (670.5 μA mM^{-1} cm^{-2}). Moreover, the detection limit (0.08 μM) is lower than that (0.15 μM) of Co_3O_4. Importantly, what inspired us is that the comprehensive analytical parameters of the CTAB–Co_3O_4 electrode will be the best values for non-enzymatic glucose sensors based on cobalt oxide.[14,15,26,27] Furthermore, the sensitivity, linear range as well as the detection limit obtained from the CTAB–Co_3O_4 electrode are among the best reported values for non-enzymatic sensors based on some other nanostrucures.[9,28–31]The significant improvement may be attributed to the fact that the free-standing nanofibers and the 3D electrode structure can provide enhanced active sites for the electrocatalytic reaction and construct many highways for the transport of ions and molecules.

Good selectivity is very important and challenging for non-enzymatic glucose sensors since easily oxidized species such as ascorbic acid (AA) and uric acid (UA) normally co-exist with glucose in human blood. The normal physiological level of glucose is 4–7 mM, and the concentrations of other oxidative species are less than 0.1 mM, respectively. Therefore, mixed solutions of 0.1 mM AA and 1 mM glucose, 0.1 mM fructose and 1 mM glucose or 0.1 mM UA and 1 mM glucose were tested, respectively, for investigating the selectivity of the CTAB–Co_3O_4 electrode. According to the results presented in Fig. 3A and the inset, 0.1 mM AA, 0.1 mM fructose and 0.1 mM UA only induce a 4.7%, 1.7% and 2.8% current increase, respectively, compared with 1 mM glucose. The good selectivity can be hypothesized as the repelling effect as well as the more negative potential mentioned above. Co_3O_4 has an isoelectric point (IEP) of ~8. In the electrolyte of 0.5 M NaOH, Co_3O_4 is negatively charged and the UA and AA are also negatively charged due to the loss of protons in the presence of hydroxy ions. Consequently, the

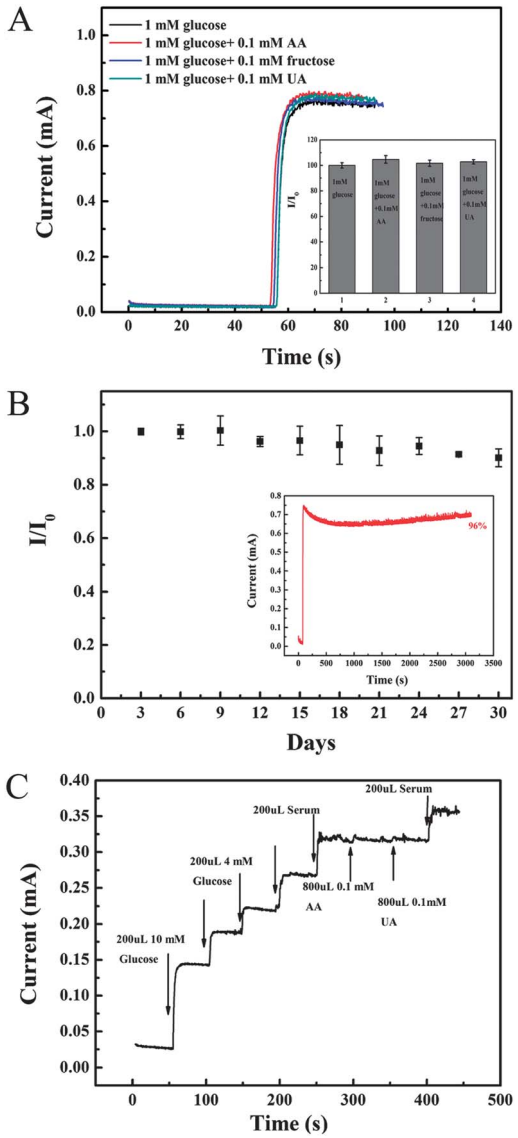

Fig. 3 (A) Current response of CTAB–Co_3O_4 electrode to 1 mM glucose, 1 mM glucose + 0.1 mM AA, 1 mM glucose + 0.1 mM fructose, and 1 mM glucose + 0.1 mM UA, respectively. Inset shows the comparison of current response of test analytes; (B) normalized sensitivity of the CTAB–Co_3O_4 electrode to glucose tested every three days by amperometric measurement over 30 consecutive days. Inset shows the amperometric response towards 1.0 mM glucose over a long time-period of 3000 s; (C) amperometric response of the CTAB–Co_3O_4 electrode with successive additions of different of analytes.

electrocatalysis of Co_3O_4 towards UA and AA oxidation can be reduced by the charge repelling effect.[32]

The reproducibility and stability of the CTAB–Co_3O_4 electrode was also evaluated. The relative standard deviation (R.S.D.) of 3.7% ($n = 5$) for 0.5 mM glucose demonstrated the good intra-electrode reproducibility. The good inter-electrode reproducibility was characterized by the low R.S.D. of 6.3% in the response to 1 mM glucose on four CTAB–Co_3O_4 electrodes. Additionally, the long-term stability is also an important parameter of evaluating the performance of a glucose sensor. As shown in the inset of the Fig. 3B, only 4% current signal is lost over a long period of 3000 s. The stability of the proposed glucose sensor was also tested by measuring the current response to 0.5 mM glucose at intervals of three days when the CTAB–Co_3O_4 electrode was stored in air at an ambient environment. The current response of the sensor maintains 90% of the initial value after one month (Fig. 3B). These results suggest the sensors based on the CTAB–Co_3O_4 electrode have good reproducibility and stability.

The applicability was tested by determining the glucose concentration in human serum samples. Firstly, the electrocatalytic property of the CTAB–Co_3O_4 electrode towards the glucose in human serum was investigated by cyclic voltammetry as shown in Fig. S3.† The result shows that the electrode demonstrates high electrocatalytic ability for glucose oxidation in human serum, which provides the possibility for the detection of glucose in human serum. Fig. 3C demonstrated the successive addition of the analytes (standard glucose, human serum sample, AA and UA). The concentration of glucose in the human serum sample was calculated using standard glucose solution and the result is presented in Table S1 of the ESI.† The results tested using the CTAB–Co_3O_4 electrode are in agreement with those read from a commercial GOD-based sensor. Furthermore, the addition of the 0.1 mM AA and 0.1 mM UA cause insignificant signal and would not affect glucose detection in real samples.

The 3D electrode decorated with Co_3O_4 microspheres with free-standing nanofibers was constructed and applied for the detection of glucose. The enhanced electrocatalytic activity towards glucose oxidation including its low potential, fast response time, wide linear range, high sensitivity, good selectivity as well as long-term stability had been obtained. In particular, the electrode showed comparable application with a commercial glucose oxidase (GOD)-based sensor. All these results suggest that the 3D electrode decorated with Co_3O_4 microspheres with free-standing nanofibers could be potentially applied for the construction of a non-enzymatic sensor.

This work was supported by grants from the National Natural Science Foundation of China (NNSFC no. 20903050), the Fundamental Research Funds for the Central University (Lzujbky-2012-22 and Lzujbky-2012-79) and the National Science Foundation for Fostering Talents in Basic Research of the National Natural Science Foundation of China (Grant no. J1103307 and 20130730096). LZUMMM2013004 and the Science and Technology Program of Gansu Province of China (1107RJYA004).

Notes and references

1 A. Safavi, N. Maleki and E. Farjami, *Biosens. Bioelectron.*, 2009, **24**, 1655–1660.
2 H.-B. Noh, K. S. Lee, P. Chandra, M. S. Won and Y. B. Shim, *Electrochim. Acta*, 2012, **61**, 36–43.
3 P. Si, Y. Huang, T. Wang and J. Ma, *RSC Adv.*, 2013, **3**, 3487–3502.
4 Y. Ma, J. Di, X. Yan, M. Zhao, Z. Lu and Y. Tu, *Biosens. Bioelectron.*, 2009, **24**, 1480–1483.
5 J. Lu, I. Do, L. T. Drzal, R. M. Worden and I. Lee, *ACS Nano*, 2008, **2**, 1825–1832.
6 W. Chen, S. Cai, Q. Q. Ren, W. Wen and Y. D. Zhao, *Analyst*, 2012, **137**, 49–58.

7 X. Zhang, A. Gu, G. Wang, Y. Wei, W. Wang, H. Wu and B. Fang, *CrystEngComm*, 2010, **12**, 1120–1126.
8 X. Zhou, H. Nie, Z. Yao, Y. Dong, Z. Yang and S. Huang, *Sens. Actuators, B*, 2012, **168**, 1–7.
9 Y. Ding, Y. Liu, J. Parisi, L. Zhang and Y. Lei, *Biosens. Bioelectron.*, 2011, **28**, 393–398.
10 L. Li, Y. Li, S. Gao and N. Koshizaki, *J. Mater. Chem.*, 2009, **19**, 8366–8371.
11 L. Li, T. Sasaki, Y. Shimizu and N. Koshizaki, *J. Phys. Chem. C*, 2009, **113**, 15948–15954.
12 X. He, Y. Wu, F. Zhao, J. Wang, K. Jiang and S. Fan, *J. Mater. Chem. A*, 2013, **1**, 11121–11125.
13 X. Liu, Q. Long, C. Jiang, B. Zhan, C. Li, S. Liu, Q. Zhao, W. Huang and X. Dong, *Nanoscale*, 2013, **5**, 6525–6529.
14 Y. Ding, Y. Wang, L. Su, M. Bellagamba, H. Zhang and Y. Lei, *Biosens. Bioelectron.*, 2010, **26**, 542–548.
15 C. W. Kung, C. Y. Lin, Y. H. Lai, R. Vittal and K. C. Ho, *Biosens. Bioelectron.*, 2011, **27**, 125–131.
16 X. C. Dong, H. Xu, X. W. Wang, Y. X. Huang, M. B. Chan Park, H. Zhang, L.-H. Wang, W. Huang and P. Chen, *ACS Nano*, 2012, **6**, 3206–3213.
17 Z. Luo, S. Yin, K. Wang, H. Li, L. Wang, H. Xu and J. Xia, *Mater. Chem. Phys.*, 2012, **132**, 387–394.
18 G. W. Yang, C. L. Xu and H. L. Li, *Chem. Commun.*, 2008, 6537–6539.
19 Y. M. Wang, D. D. Zhao, Y. Q. Zhao, C. L. Xu and H. L. Li, *RSC Adv.*, 2012, **2**, 1074–1082.
20 C. Guo, Y. Wang, Y. Zhao and C. Xu, *Anal. Methods*, 2013, **5**, 1644–1647.
21 W. Lu, X. Qin, A. M. Asiri, A. O. Al Youbi and X. Sun, *Analyst*, 2013, **138**, 417–420.
22 J. Y. Xiang, J. P. Tu, L. Zhang, Y. Zhou, X. L. Wang and S. J. Shi, *Electrochim. Acta*, 2010, **55**, 1820–1824.
23 Y. Wang, W. Wang and W. Song, *Electrochim. Acta*, 2011, **56**, 10191–10196.
24 M. G. Innocenzo and G. Casella, *J. Electroanal. Chem.*, 2002, **534**, 31–38.
25 J. Yang, W. d. Zhang and S. Gunasekaran, *Electrochim. Acta*, 2011, **56**, 5538–5544.
26 C. Hou, Q. Xu, L. Yin and X. Hu, *Analyst*, 2012, **137**, 5803–5808.
27 H. Pang, F. Gao, Q. Chen, R. Liu and Q. Lu, *Dalton Trans.*, 2012, **41**, 5862–5868.
28 W. Lv, F. M. Jin, Q. Guo, Q. H. Yang and F. Kang, *Electrochim. Acta*, 2012, **73**, 129–135.
29 Z. Zhuang, X. Su, H. Yuan, Q. Sun, D. Xiao and M. M. F. Choi, *Analyst*, 2008, **133**, 126–132.
30 S. Liu, J. Tian, L. Wang, X. Qin, Y. Zhang, Y. Luo, A. M. Asiri, A. O. Al-Youbi and X. Sun, *Catal. Sci. Technol.*, 2012, **2**, 813–817.
31 Q. Wang, X. Cui, J. Chen, X. Zheng, C. Liu, T. Xue, H. Wang, Z. Jin, L. Qiao and W. Zheng, *RSC Adv.*, 2012, **2**, 6245–6249.
32 Y. Ding, Y. Wang, L. Su, H. Zhang and Y. Lei, *J. Mater. Chem.*, 2010, **20**, 9918.